Structure and dynamics of the polar antiferromagnets $Ni_{3-x}Co_xTeO_6$ (x=1,2)

Supplemental Materials

Stella Skiadopoulou,[1,2,3] Maria Retuerto,[3] Fedir Borodavka,[1] Christelle Kadlec,[1] Filip Kadlec,[1] Martin Míšek[1], Jan Prokleška,[5] Zheng Deng,[4] Xiaoyan Tan,[4ξ] Corey Frank,[4] Jose A. Alonso,[6] Maria Tereza Fernandez-Diaz,[7] Mark Croft,[8] Fabio Orlandi,[9] Pascal Manuel,[9] Emma McCabe,[10] Dominik Legut,[2] Martha Greenblatt[4] and Stanislav Kamba[1]

[1]*Institute of Physics,Czech Academy of Sciences, Na Slovance 2, 18221 Prague 8, Czech Republic*
[2]*IT4Innovations, VSB Technical University of Ostrava, 17. listopadu 15, CZ-708 33 Ostrava-Poruba, Czech Republic*
[3]*School of Physics, CRANN, Trinity College, Dublin 2, Ireland*
[4]*Department of Chemistry and Chemical Biology, Rutgers, The State University of New Jersey, 610 Taylor Road, Piscataway, NJ 08854, USA*
[5]*Department of Condensed Matter Physics, Faculty of Mathematics and Physics, Charles University, Ke Karlovu 5, 121 16 Prague 2, Czech Republic*
[6]*Instituto de Ciencia de Materiales de Madrid, C.S.I.C., Cantoblanco, E-28049 Madrid, España.*
[7]*Institut Laue Langevin, BP 156X, Grenoble, F-38042, France*
[8]*Department of Physics and Astronomy, Rutgers, the State University of New Jersey, 136 Frelinghusen Road, Piscataway, NJ 08854, USA*
[9]*ISIS Facility, STFC, Rutherford Appleton Laboratory, Chilton, Didcot, Oxfordshire, OX11 0QX, UK*
[10]*School of Physical Sciences, University of Kent, Canterbury, Kent, CT2 7NH, UK*
[ξ] *Current address: Department of Chemistry and Biochemistry, George Mason University, 4400 University Dr, Fairfax, VA 22030*

CONTENTS

S1. Single crystal synthesis

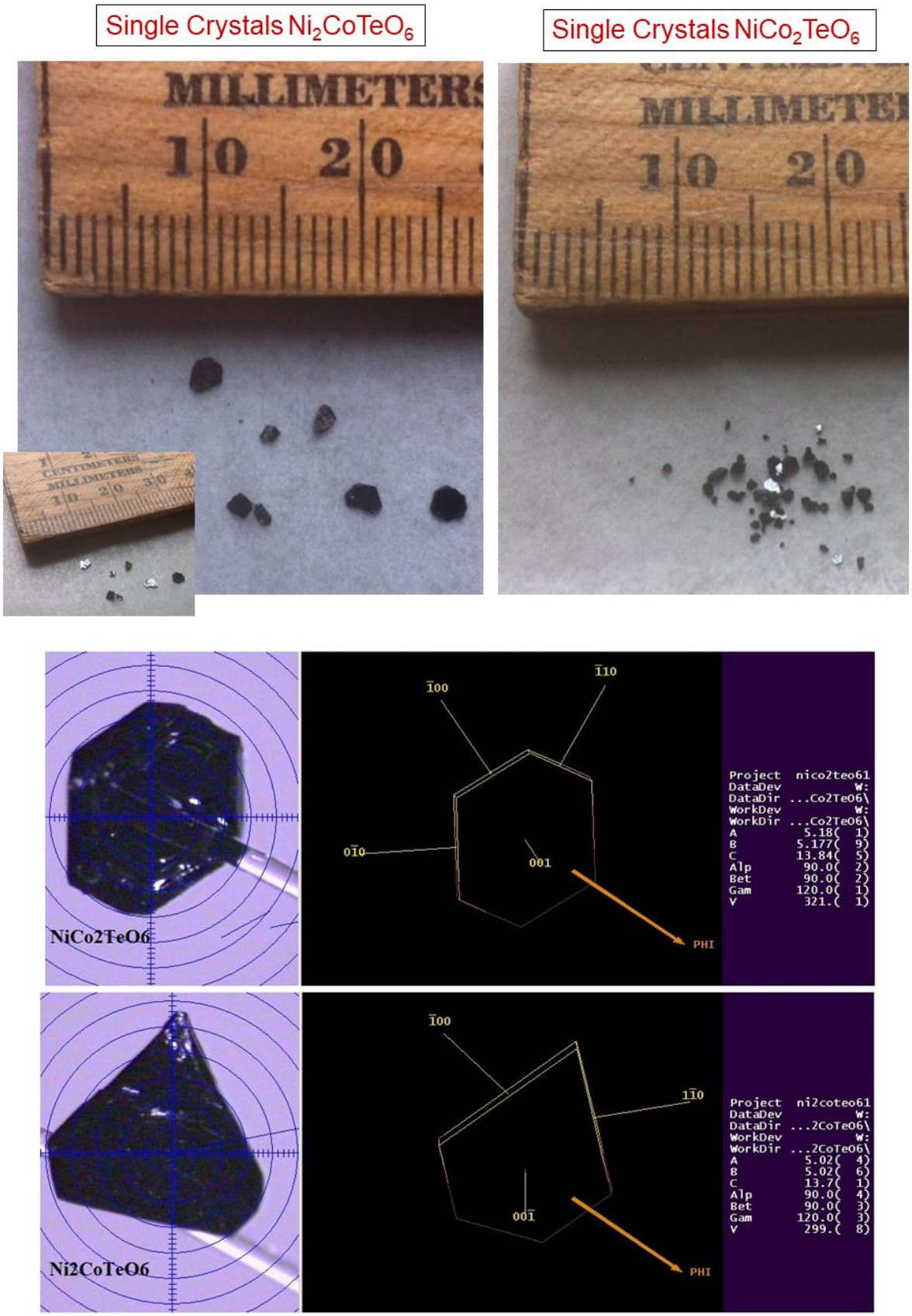

Figure S1.1 Images of Ni_2CoTeO_6 and $NiCo_2TeO_6$ single crystals and their orientation.

S2. X-Ray Diffraction

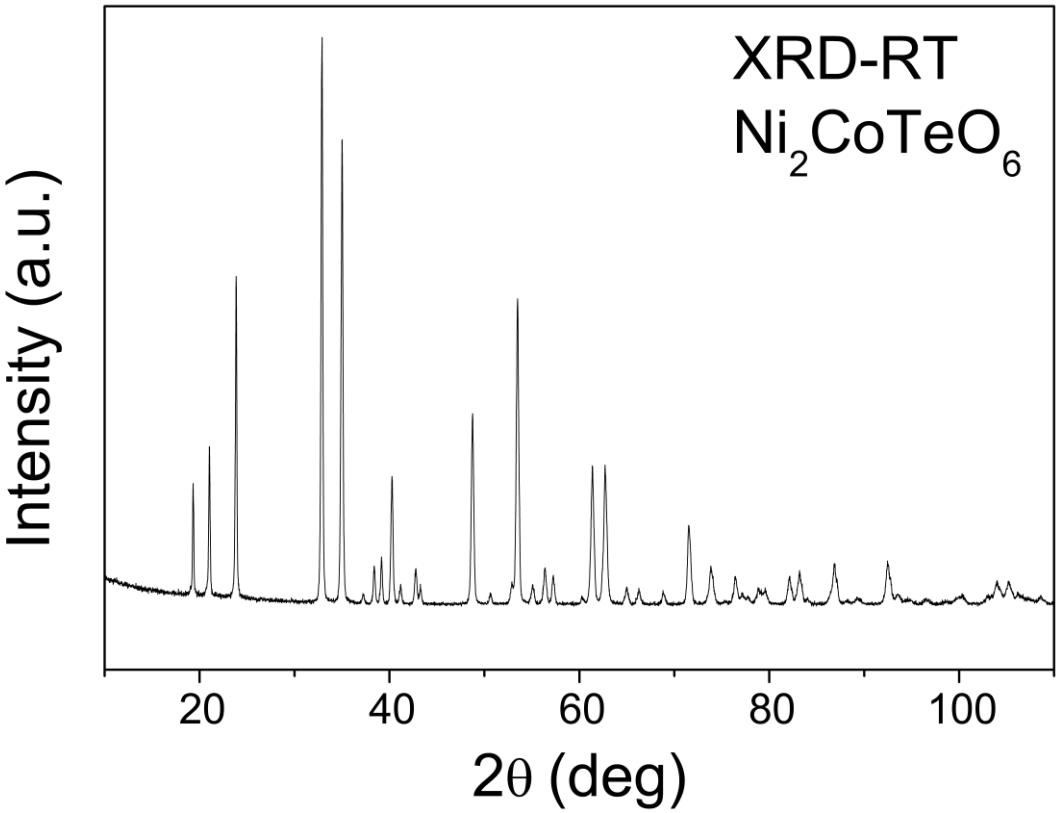

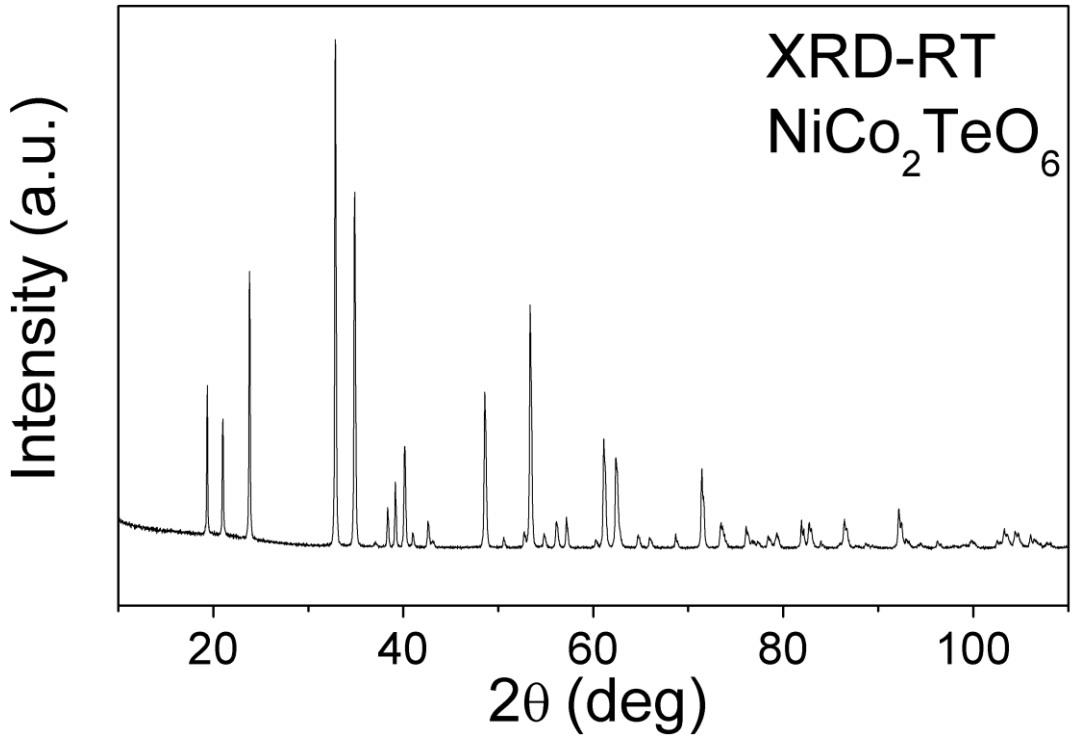

Figure S2.1 X-Ray Diffraction patterns of Ni_2CoTeO_6 and $NiCo_2TeO_6$ at room temperature.

S3. Neutron Powder Diffraction

S3.1 $Ni_2CoTeO6$ and $NiCo_2TeO_6$ in paramagnetic region.

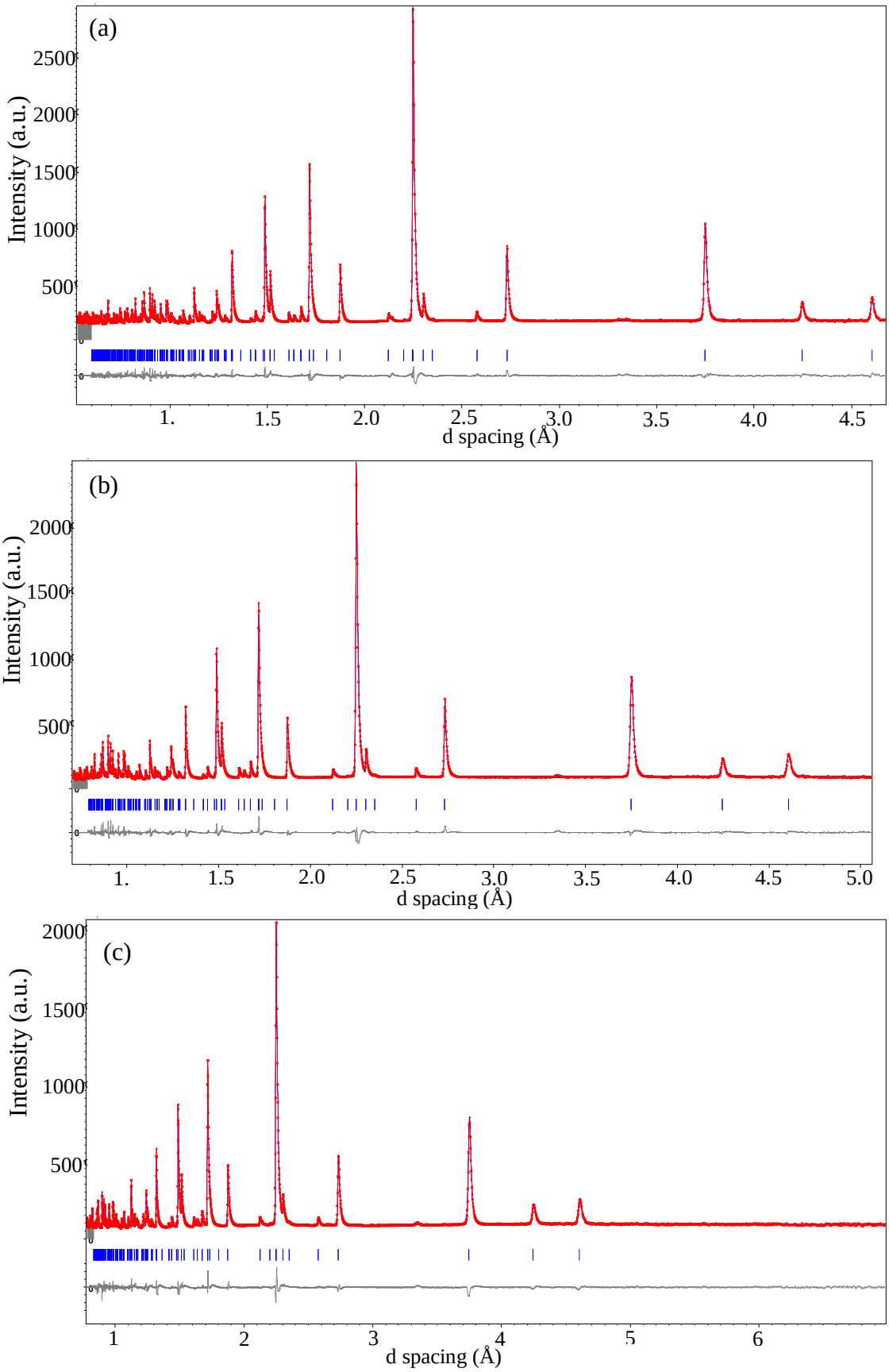

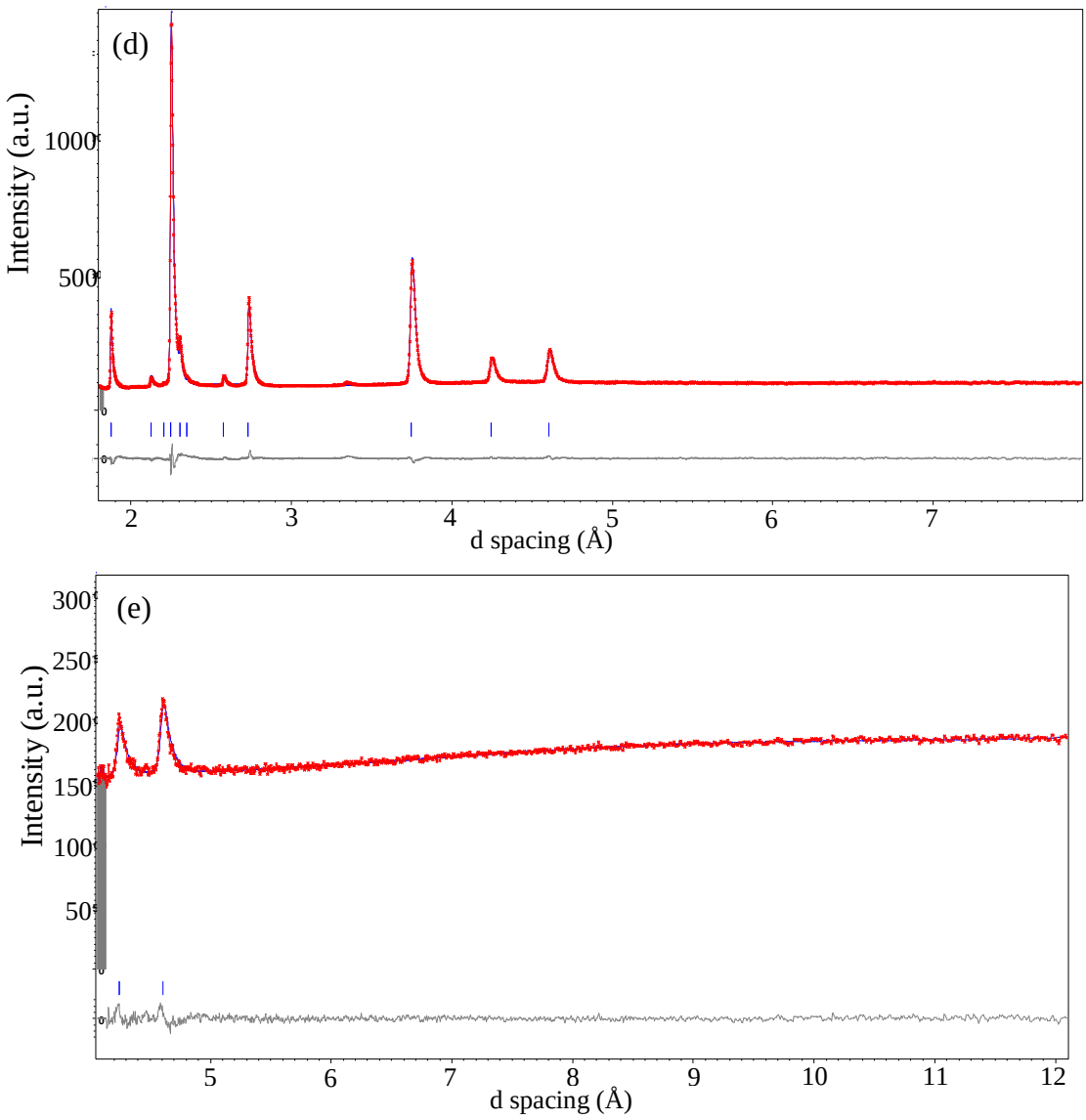

Figure S3.1.1 Rietveld refinement profiles for NiCo2TeO6 using time-of-flight NPD data collected at 60 K showing observed, calculated and different profiles in red, blue and grey, respectively (blue ticks show positions of peaks for the main phase); (a) shows bank 5 (153°) data, (b) shows bank 4 (122°) data, (c) shows bank 3 (90°) data, (d) shows bank 2 (58°) data and (e) shows bank 1 (27°) data; Rwp = 3.52%, Rp = 2.81% and $\chi 2$ = 7.90.

Table S3.1.1 Refinement details from refinement using 60 K NPD data for $NiCo_2TeO_6$ in space group *R*3 (cations on the 3*a* site (0, 0, *z*)), *a* = 5.15218(1) Å, *c* = 13.81581(9) Å, R_{wp} = 3.52%, R_p = 2.81% and χ^2 = 7.90.

Atom	**Site**	***x***	***y***	***z***	**U_{iso} × 100 (Å^2)**	**occupancy**
Ni/Co(1)	3*a*	0	0	0.3053(2)	1.15(1)†	0.559(4)/0.441(4)
Ni/Co(2)	3*a*	0	0	0.5071(8)	1.15(1)†	0/1
Ni/Co(3)	3*a*	0	0	0.7934(3)	1.15(1)†	0.441(4)/0.559(4)
Te	3*a*	0	0	0*	1.15(1)†	1
O(1)	9*b*	-0.0285(3)	0.3285(2)	0.2414(3)	2.72(9)	1
O(2)	9*b*	0.6474(3)	-0.0444(3)	0.0700(2)	1.21(6)	1

*fixed at zero to define unit cell origin along polar *c* axis
†cation U_{iso} values constrained to be equal

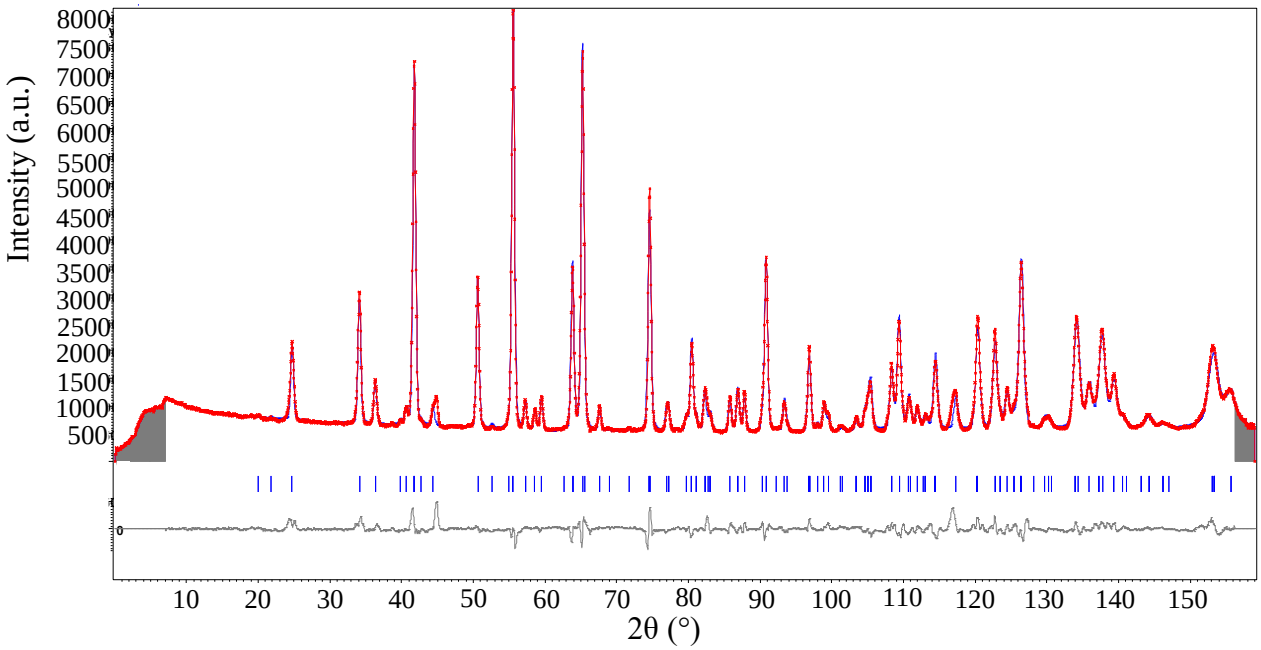

Figure S3.1.2 Rietveld refinement profiles for Ni_2CoTeO_6 using constant wavelength NPD data (collected on D2B) collected at 300 K showing observed, calculated and different profiles in red, blue and grey, respectively; R_{wp} = 5.72%, R_p = 3.93% and χ^2 = 13.32.

Table S3.1.2 Refinement details from refinement using 300 K NPD (D2B) data for Ni_2CoTeO_6 in space group *R*3 (cations on the 3*a* site (0, 0, *z*)), *a* = 5.11516(5) Å, *c* = 13.7680(2) Å, R_{wp} = 5.72%, R_p = 3.93% and χ^2 = 13.32.

Atom	**Site**	***x***	***y***	***z***	**U_{iso} × 100 (Å^2)**	**occupancy**
Ni/Co(1)	3*a*	0	0	0.3084(4)	0.80(3)†	0.769(4)/0.231(4)
Ni/Co(2)	3*a*	0	0	0.5191(8)	0.80(3)†	0.462(8)/0.537(8)
Ni/Co(3)	3*a*	0	0	0.8064(5)	0.80(3)†	0.769(4)/0.231(4)
Te	3*a*	0	0	0*	1.8(1)	1
O(1)	9*b*	-0.011(1)	0.351(1)	0.2441(5)	1.50(9)	1
O(2)	9*b*	0.6351(9)	-0.043(1)	0.0776(5)	1.24(9)	1

*fixed at zero to define unit cell origin along polar *c* axis
†cation U_{iso} values constrained to be equal

Table S3.1.3 Selected bond lengths and interatomic distances from refinement using 300 K NPD (D2B) data for Ni_2CoTeO_6.

Bond	**Bond length (Å)**	**Bond**	**Bond length (Å)**
Ni/Co(1) – O(1)	3 × 2.02(8)	Te – O(1)	3 × 2.024(7)
Ni/Co(1) – O(2)	3 × 2.070(9)	Te – O(2)	3 × 2.064(6)
Ni/Co(2) – O(1)	3 × 1.874(8)	Ni/Co(1) – Ni/Co(2)	2.90(1)
Ni/Co(2) – O(2)	3 × 2.124(9)	Ni/Co(2) – Ni/Co(3)	3.021(2)
Ni/Co(3) – O(1)	3 × 2.157(8)	Te – Ni/Co(3)	2.666(7)
Ni/Co(3) – O(2)	3 × 2.039(7)		

S3.2 $Ni_2CoTeO6$ and $NiCo_2TeO_6$ below T_N.

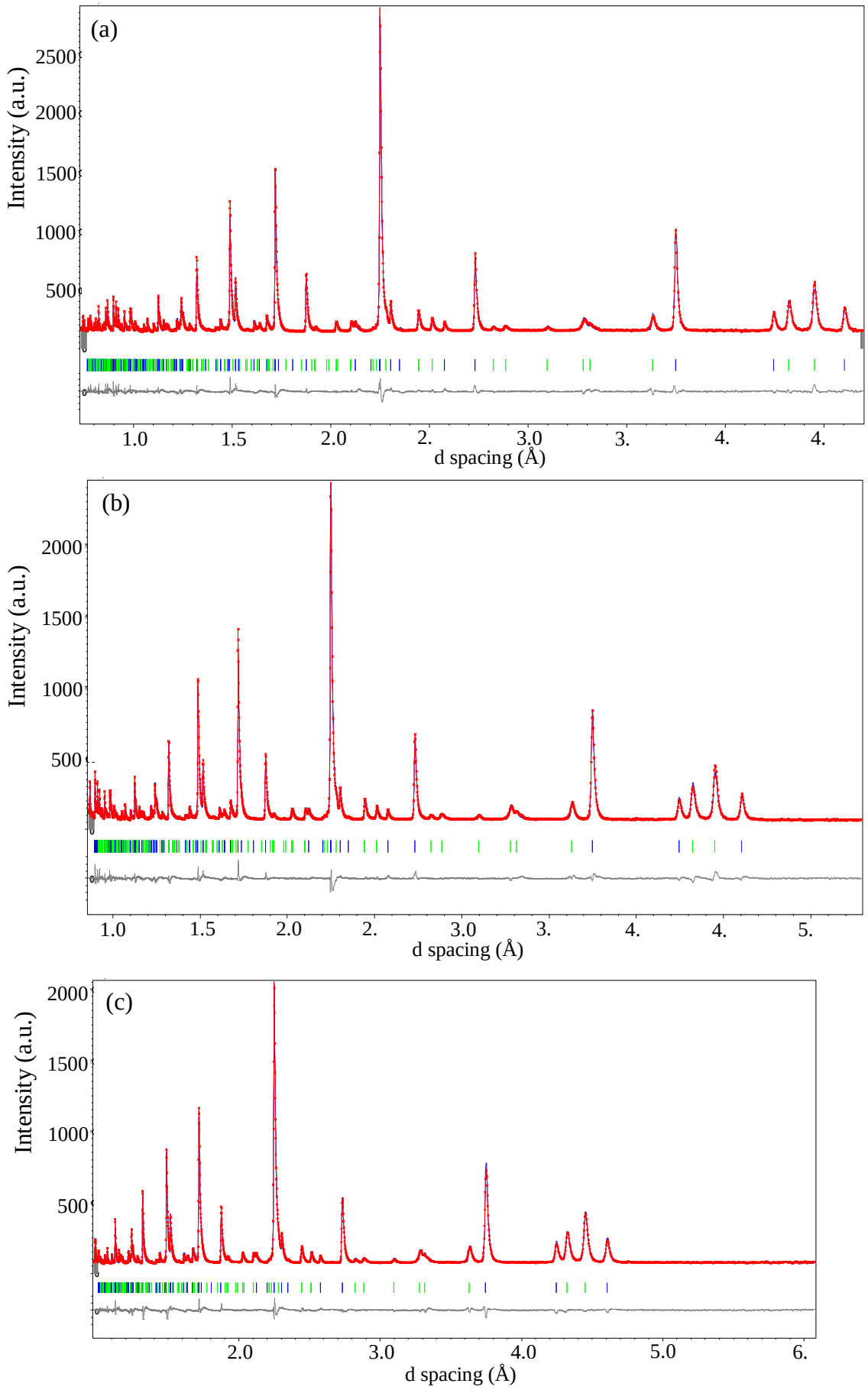

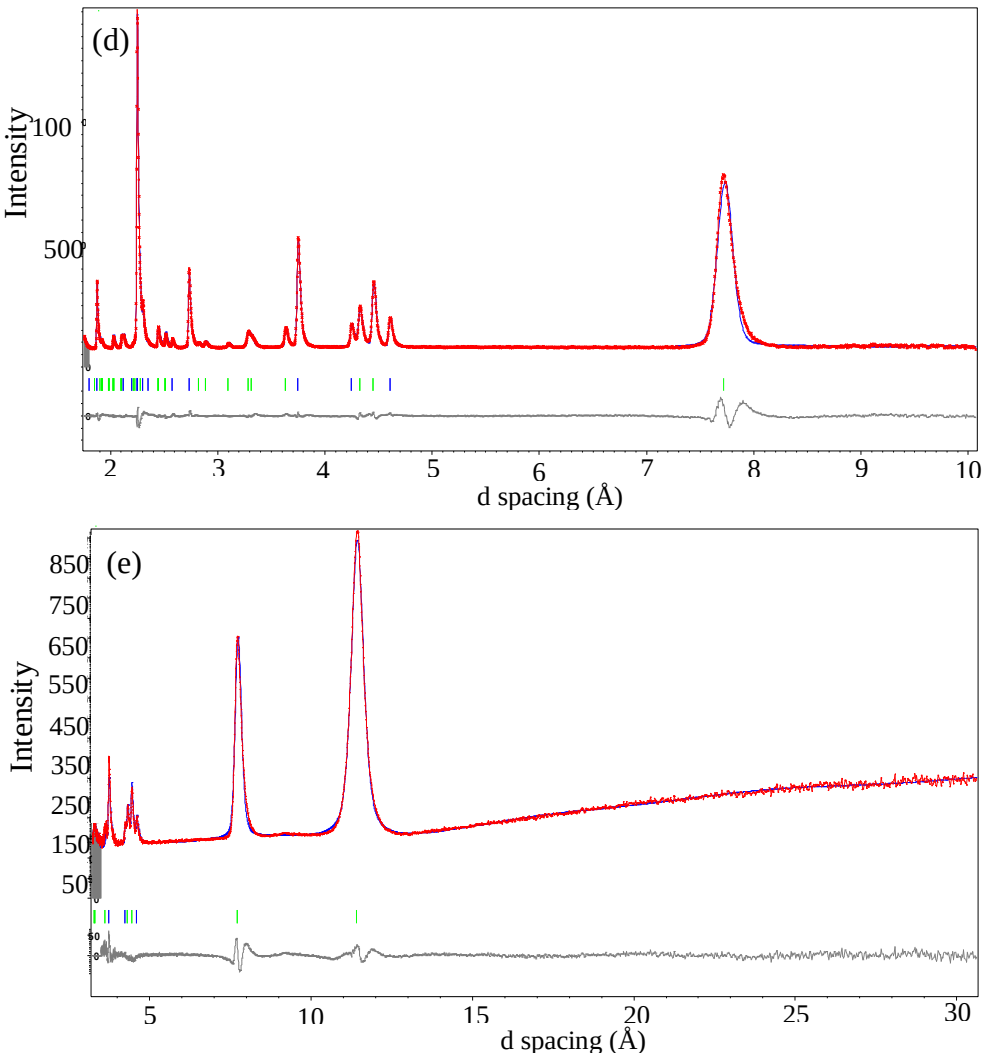

Figure S3.2.1 Rietveld refinement profiles for $NiCo_2TeO_6$ using time-of-flight NPD data collected at 1.5 K showing observed, calculated and different profiles in red, blue and grey, respectively (blue ticks show positions of peaks for the main phase); (a) shows bank 5 (153°) data, (b) shows bank 4 (122°) data, (c) shows bank 3 (90°) data, (d) shows bank 2 (58°) data and (e) shows bank 1 (27°) data; R_{wp} = 4.24%, R_p = 3.27% and χ^2 = 12.04.

Table S3.2.1 Refinement details from refinement using 1.5 K NPD data for $NiCo_2TeO_6$ in space group *R*3 (cations on the 3*a* site (0, 0, *z*)), *a* = 5.15069(2) Å, *c* = 13.8125(1) Å, magnetic propagation vector *q* = (0 0 1.2110(1)); R_{wp} = 4.24%, R_p = 3.27% and χ^2 = 12.04.

Atom	Site	*x*	*y*	*z*	U_{iso} × 100 (Å^2)	occupancy	μ (μ_B)
Ni/Co(1)	3*a*	0	0	0.3051(1)	1.83(1)†	0.56/0.44	2.63(3)††
Ni/Co(2)	3*a*	0	0	0.5104(4)	1.83(1)†	0/1	3.20(5)
Ni/Co(3)	3*a*	0	0	0.7922(2)	1.83(1)†	0.44/0.56	2.63(3)††
Te	3*a*	0	0	0*	1.83(1)†	1	
O(1)	9*b*	-0.0339(3)	0.3295(3)	0.2316(2)	1.83(1)†	1	
O(2)	9*b*	0.6506(3)	-0.0439(3)	0.0588(2)	1.83(1)†	1	

*fixed at zero to define unit cell origin along polar *c* axis

† U_{iso} values constrained to be equal

†† Moments for sites (1) and (3) were constrained to be equal to overcome correlation issues in the refinement; note the similar site occupancies for these two sites.

Table S3.2.2 Selected bond lengths and interatomic distances from refinement using 1.5 K time-of-flight NPD data for $NiCo_2TeO_6$.

Bond	Bond length (Å)	Bond	Bond length (Å)
Ni/Co(1) – O(1)	3 × 2.059(3)	Te – O(1)	3 × 2.094(3)
Ni/Co(1) – O(2)	3 × 1.975(3)	Te – O(2)	3 × 1.882(3)
Ni/Co(2) – O(1)	3 × 1.969(3)	Ni/Co(1) – Ni/Co(2)	2.836(6)
Ni/Co(2) – O(2)	3 × 2.264(5)	Ni/Co(2) – Ni/Co(3)	3.056(1)
Ni/Co(3) – O(1)	3 × 2.129(4)	Te – Ni/Co(3)	2.862(3)
Ni/Co(3) – O(2)	3 × 2.118(3)		

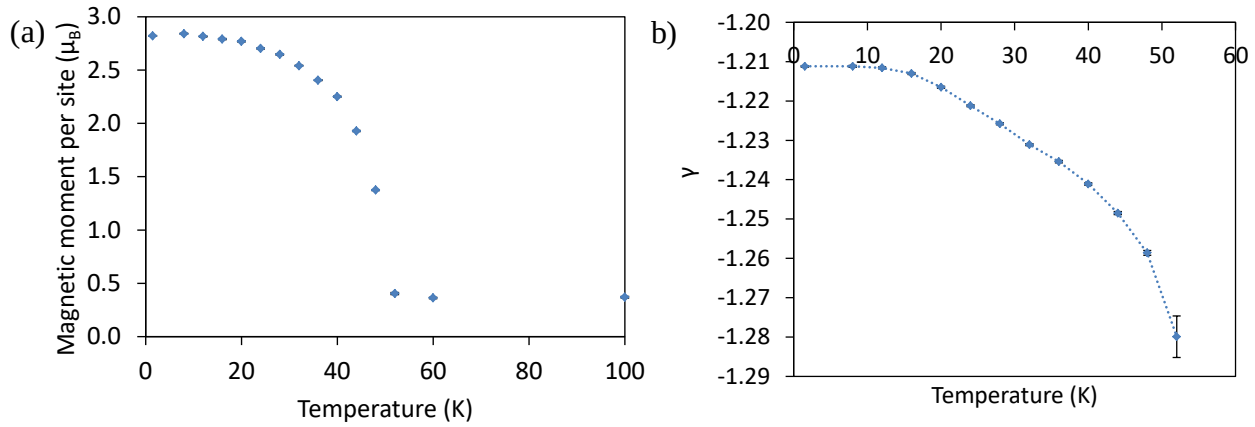

Figure S3.2.2 (a) average magnetic moment per Ni/Co site as a function of temperature and (b) evolution of magnetic propagation vector component γ *k*=(0 0 γ) with temperature for $NiCo_2TeO_6$ from sequential Rietveld refinements using time-of-flight NPD data (bank 3 data).

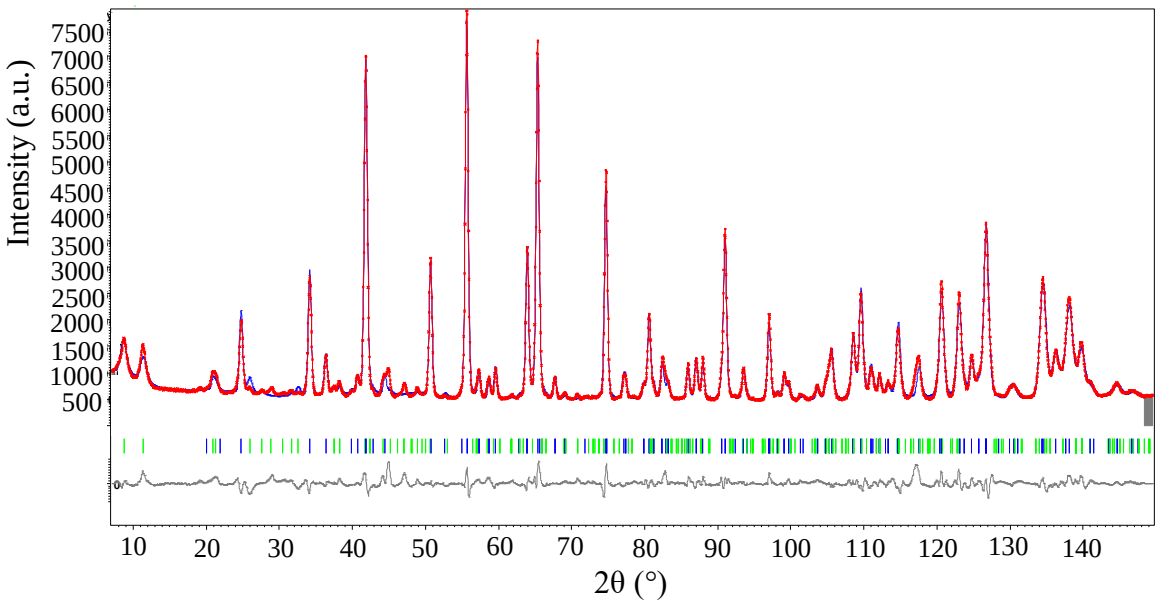

Figure S3.2.3 Rietveld refinement profiles for Ni_2CoTeO_6 using constant wavelength NPD data (collected on D2B) collected at 3 K showing observed, calculated and different profiles in red, blue and grey, respectively; R_{wp} = 6.51%, R_p = 4.62% and χ^2 = 19.62.

Table S3.2.3 Refinement details from refinement using 3 K NPD (D2B) data for Ni_2CoTeO_6 in space group *R*3 (cations on the 3*a* site (0, 0, *z*)), *a* = 5.10863(5) Å, *c* = 13.7502(2) Å, magnetic propagation vector *q* = (0 0 1.299(4)); R_{wp} = 6.51%, R_p = 4.62% and χ^2 = 19.62.

Atom	Site	*x*	*y*	*z*	U_{iso} × 100 (Å^2)	occupancy	μ (μ_B)
Ni/Co(1)	3*a*	0	0	0.3077(4)	0.07(2)†	0.77/0.23	2.63(3)††
Ni/Co(2)	3*a*	0	0	0.5186(5)	0.07(2)†	0.46/0.54	2.63(3)††
Ni/Co(3)	3*a*	0	0	0.8050(5)	0.07(2)†	0.77/0.23	2.63(3)††
Te	3*a*	0	0	0*	0.07(2)†	1	
O(1)	9*b*	-0.011(1)	0.348(1)	0.2434(5)	0.07(2)†	1	
O(2)	9*b*	0.6379(9)	-0.048(1)	0.0768(5)	0.07(2)†	1	

*fixed at zero to define unit cell origin along polar *c* axis
† U_{iso} values constrained to be equal
†† Moments for sites (1) and (3) were constrained to be equal to overcome correlation issues in the refinement; note the similar site occupancies for these two sites.

Table S3.2.4 Selected bond lengths and interatomic distances from refinement using 3 K NPD (D2B) data for Ni_2CoTeO_6.

Bond	Bond length (Å)	Bond	Bond length (Å)
Ni/Co(1) – O(1)	3 × 2.012(8)	Te – O(1)	3 × 2.031(9)
Ni/Co(1) – O(2)	3 × 2.064(9)	Te – O(2)	3 × 2.036(8)
Ni/Co(2) – O(1)	3 × 1.874(8)	Ni/Co(1) – Ni/Co(2)	2.90(1)
Ni/Co(2) – O(2)	3 × 2.122(9)	Ni/Co(2) – Ni/Co(3)	3.019(2)
Ni/Co(3) – O(1)	3 × 2.164(8)	Te – Ni/Co(3)	2.681(7)
Ni/Co(3) – O(2)	3 × 2.061(8)		

S3.3 $Ni_2CoTeO6$ and $NiCo_2TeO_6$ variable temperature data.

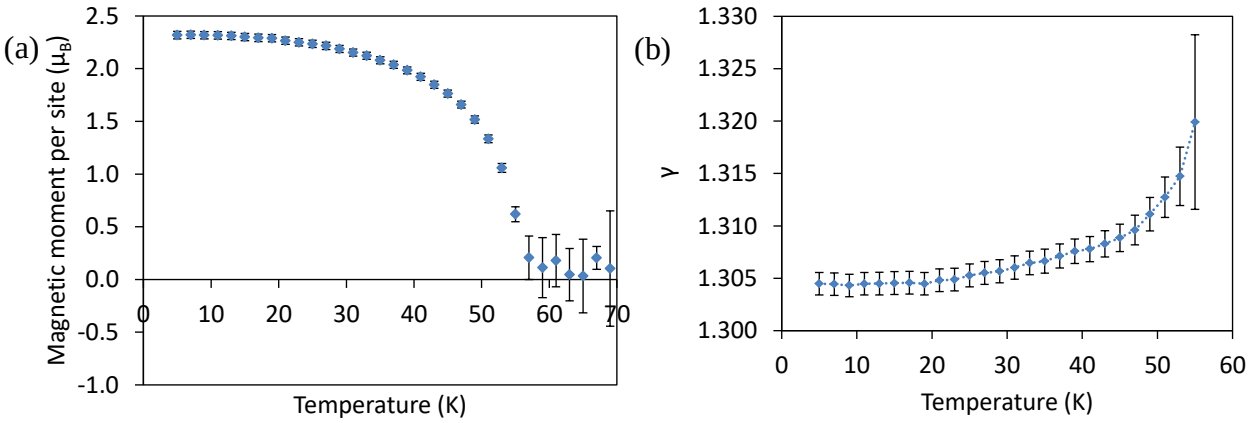

Figure S3.3 (a) average magnetic moment per Ni/Co site as a function of temperature and (b) evolution of magnetic propagation vector component γ (0 0 γ) with temperature for Ni_2CoTeO_6 from sequential Rietveld refinements using constant wavelength NPD data (D20).

S4. First-principles calculations

Spin-polarized density functional theory (DFT) calculations were conducted by the use of VASP code, implementing the projector-augmented-wave (PAW) formalism to describe the electron-ion interactions, and the Generalized Gradient Approximation parametrized by Pedrew, Burke, and Ernzerhof (GGA-PBE) for the exchange-correlation potential.[1,2] In order to compensate the magnetic moments antiferromagnetically, the hexagonal unit cell was doubled along *c*-axis (60 atoms) and sampled by Gamma-centered $8 \times 8 \times 4$ grid. The plane wave cutoff energy was set to 600 eV. Additional on-site Coulomb repulsion interactions were considered concurrently, within the rotationally invariant form of the GGA+U method (Liechtenstein approach),[3] where a Hubbard repulsion term is added for the localized 3*d* electrons (*U*) and the exchange interaction (*J*), while the other orbitals are delocalized and treated by the conventional GGA approximation.

Spin-polarized first-principles calculations, including spin-orbit coupling (SOC), were employed, aiming at investigating the structural, electronic and magnetic properties of the compounds. Within the GGA+U approach,[3] where U=7.5 eV and J=0.5 eV for both Ni and Co sites, the hexagonal lattice parameters, cell volume, band gap energy E_g, Ni and Co magnetic moments for both compounds were computed and the values are presented in Table S4.1. The hexagonal cell volume and lattice parameters are by about 3% higher than the experimental values. The estimated band gap energy E_g corresponds to 2.5 and 2.3 eV for Ni_2CoTeO_6 and $NiCo_2TeO_6$ respectively, comparable with the value of 2.2 eV for Ni_3TeO_6, as calculated by Yokosuk *et al.*.[4]

In order to investigate the magnetic ground state of the compounds, calculations of two different spin-polarized SOC magnetic structures were conducted: FM and AFM, with the spins along the *c*-axis, for a double hexagonal cell of 60 atoms, in order to represent the AFM ordering of the magnetic moments. The magnetic structures are depicted in Table S4.2. The ground sates of both compounds correspond to an AFM spin order, as seen by the total energy differences ΔE calculated by first-principles calculations.

The spin magnetic moment values per atom m_S shown in Table S4.1 remain the same for all different magnetic configurations, and lie close to the previously reported experimental ones for Ni (2 μ_B) and Co (2-2.7 μ_B), in Ni_3TeO_6[5] and Co_3TeO_6[6] respectively. The values of the orbital magnetic moment m_L for each magnetic ion are also listed in Table S4.1.

Table S4.1 Lattice parameters, cell volumes, band gap energy E_g, magnetic spin and orbital moments per atom for Ni and Co, for Ni_2CoTeO_6 and $NiCo_2TeO_6$ as obtained from the first-principles calculations. The last two columns correspond to the total energy differences with respect to the AFM magnetic ground state for each compound, hence $\Delta E_{FM} = E_{FM} - E_{AFM}$, $\Delta E_{AFM} = E_{AFM} - E_{AFM}$. The experimental values of lattice parameters and cell volumes are also displayed.

	Exper.	Calcul.	E_g (eV)	$m_{S,Ni}$ (μ_B)	$m_{S,Co}$ (μ_B)	$m_{L,Ni}$ (μ_B)	$m_{L,Co}$ (μ_B)	ΔE_{FM} (meV/f.u.)	ΔE_{AFM} (meV/f.u.)
Ni_2CoTeO_6	a=5.1257 Å c=13.7874 Å V=313.75 Å^{-3}	a=5.1649 Å c=13.9561 Å V=322.42 Å^{-3}	2.5	1.8	2.9	0.18	0.17	8.3	0
$NiCo_2TeO_6$	a=5.1606 Å c=13.8372 Å V=316.14 Å^{-3}	a=5.2106 Å c=13.9237 Å V=327.33 Å^{-3}	2.3	1.8	2.9	0.18	0.17	10.8	0

Table S4.2 Schematic representation of the different hypothetical magnetic configurations for Ni_2CoTeO_6 and $NiCo_2TeO_6$: FM (up) and AFM (down). Here only a single hexagonal cell is presented (30 atoms), whereas a double hexagonal cell (60 atoms, doubled along *c*-axis) was used for the first-principles calculations of the AFM spin-order, in order to antiferromagnetically compensate the spins. The spin chains along *c*-axis for the AFM double hexagonal setting follow the order: ↓↑↑↑↓↓ for Ni_2CoTeO_6 and ↓↓↑↑↑↑ for $NiCo_2TeO_6$. This hypothetical magnetic structure obtained from DFT calculations was not confirmed by experiment (see Fig. 1 in the main text).

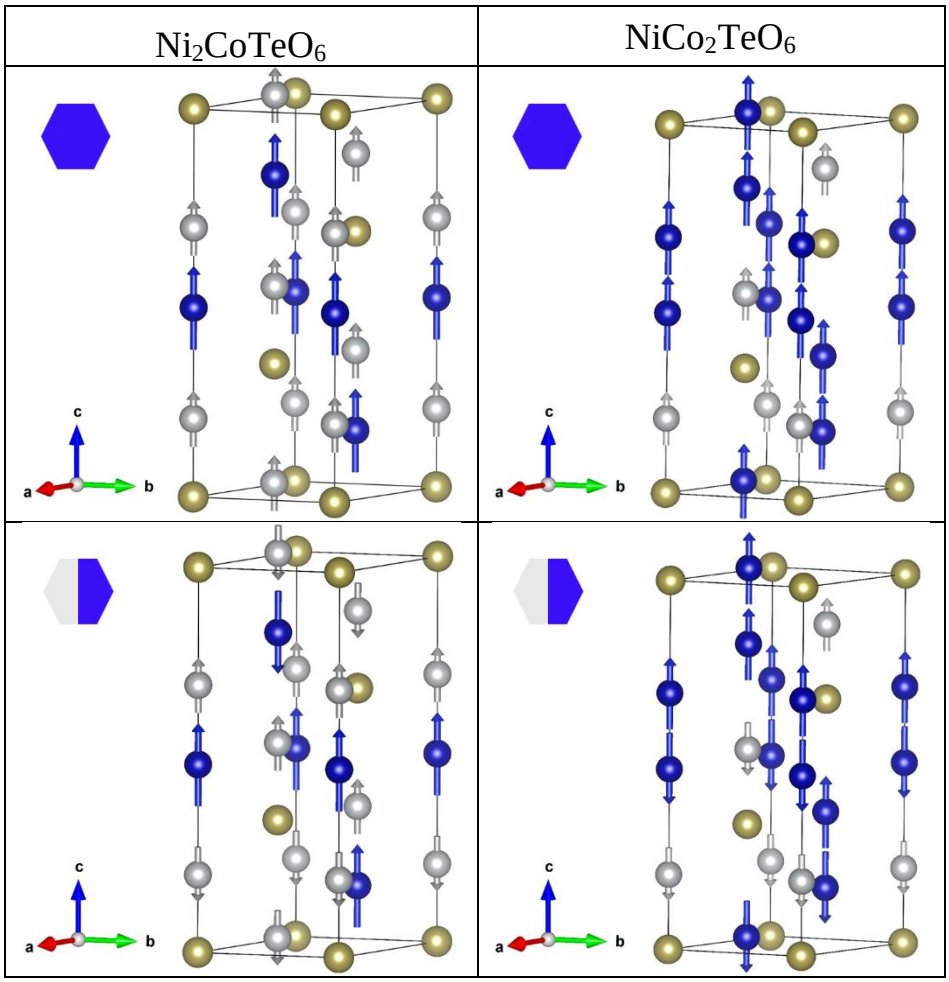

S5. Magnetic properties

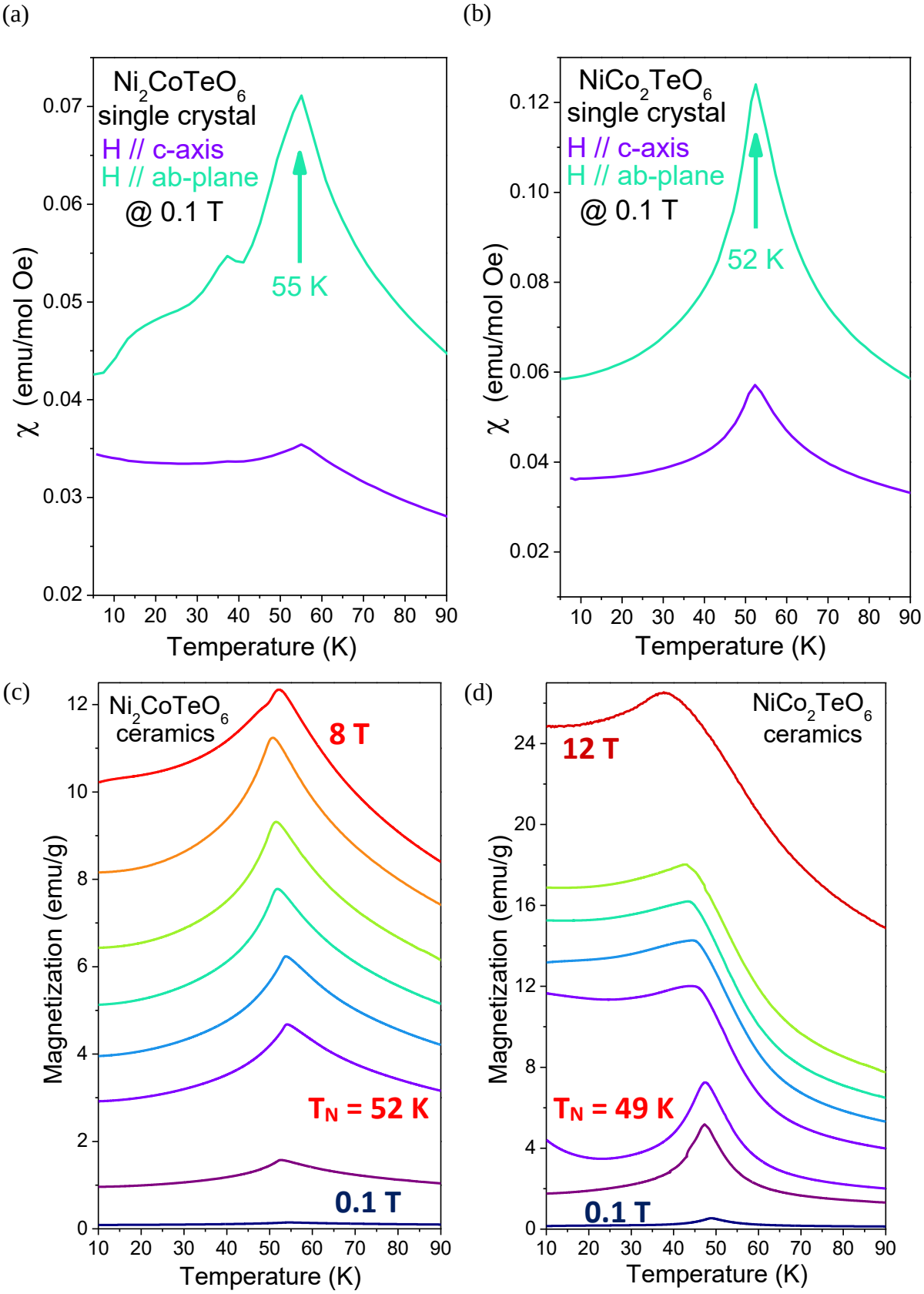

Figure S5.1 Temperature dependence of (a) Ni_2CoTeO_6 and (b) $NiCo_2TeO_6$ single crystal susceptibility at 0.1 T, for magnetic field parallel to *c*-axis and *ab*-plane. Temperature and magnetic field dependence of magnetization for (c) Ni_2CoTeO_6 and (d) $NiCo_2TeO_6$ ceramics.

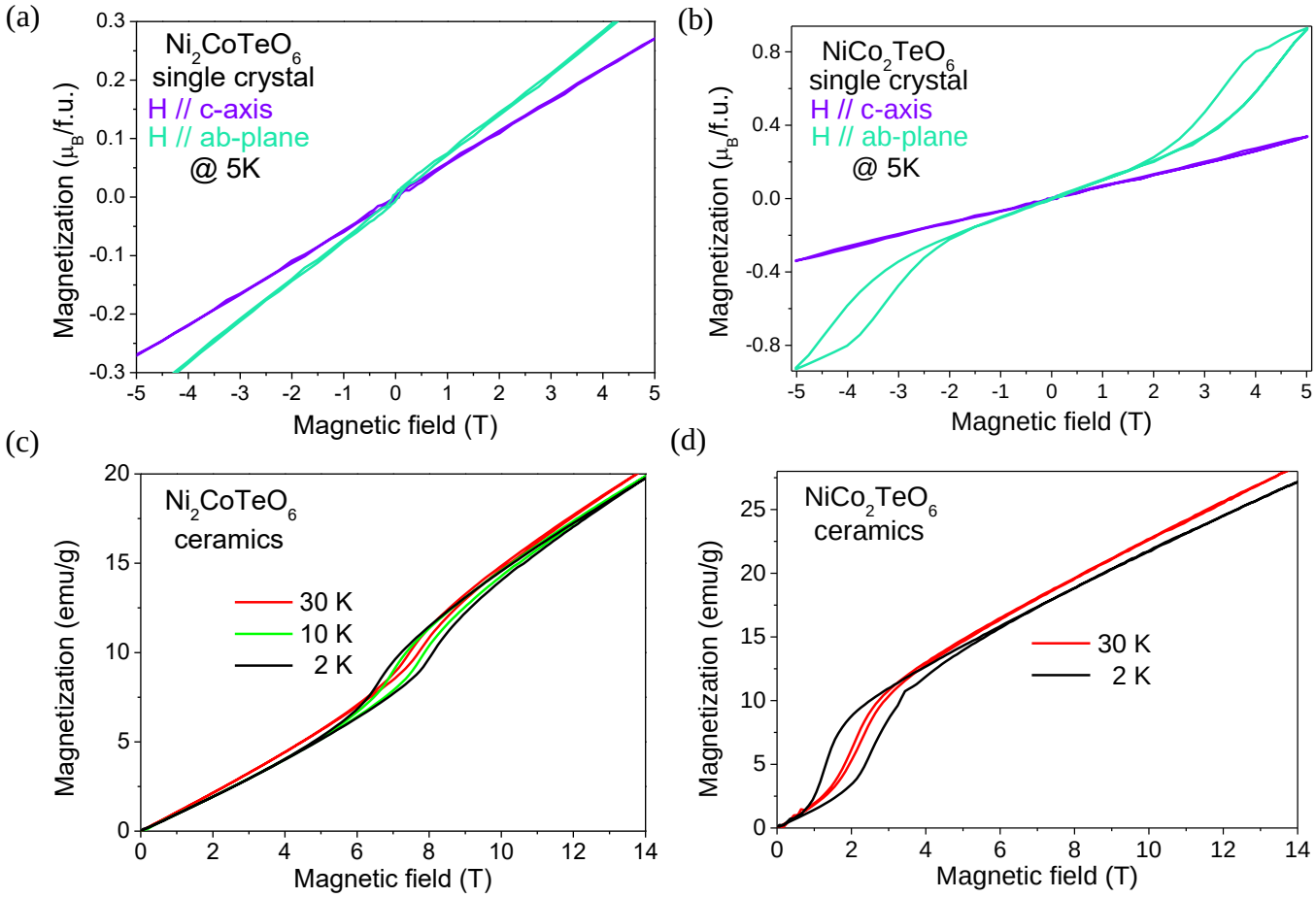

Figure S5.2 Magnetic field dependence of magnetization for (a), (c) Ni_2CoTeO_6 and (b), (d) $NiCo_2TeO_6$ single crystals and ceramics, respectively.

S6. Spin and lattice excitations

S6.1. Raman spectroscopy

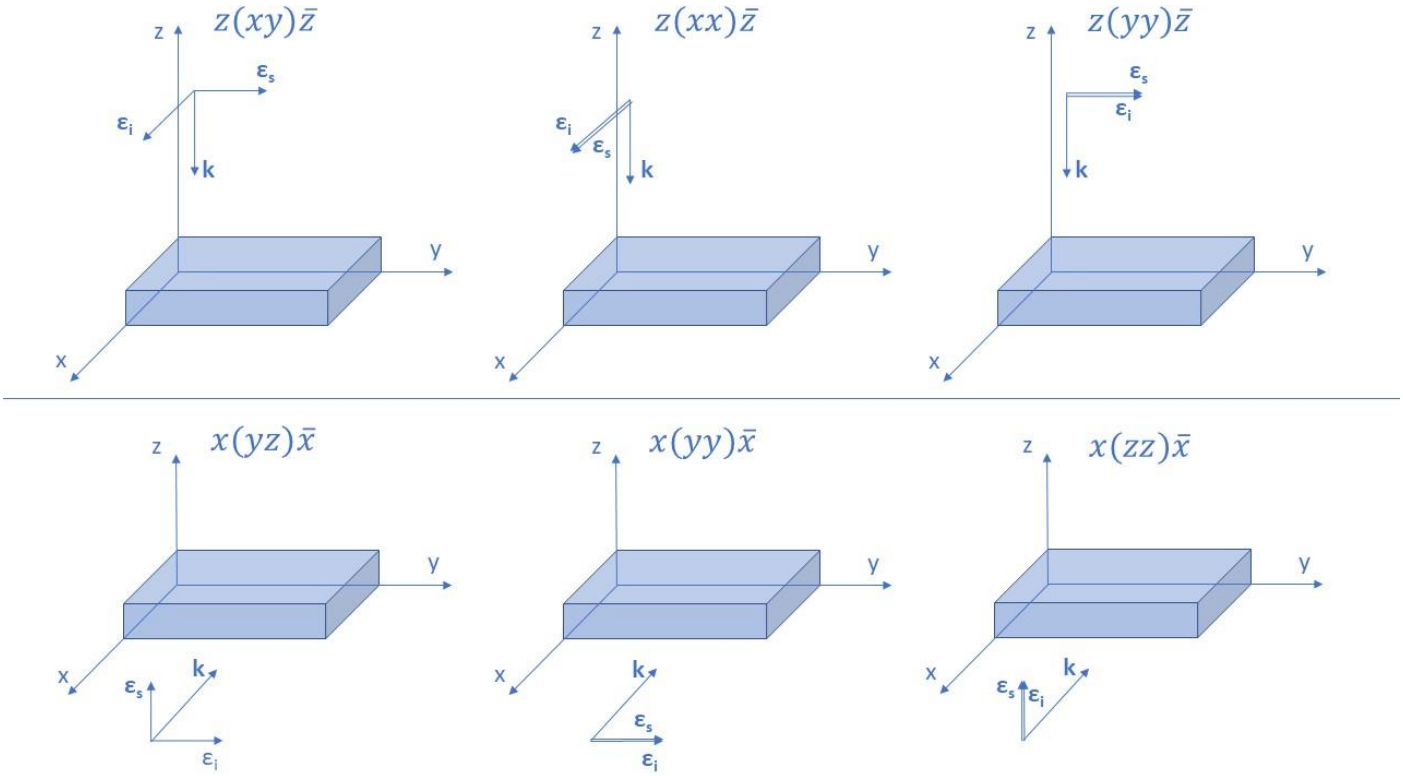

Figure S6.1.1 Experimental setup for the Raman experiments, showing the Porto notation for all possible polarization configurations in the backscattering geometry. $\boldsymbol{k}$ is the propagation vector, and, $\boldsymbol{\varepsilon_i}$ and $\boldsymbol{\varepsilon_s}$ are the polarization vectors of the incident and scattered light.

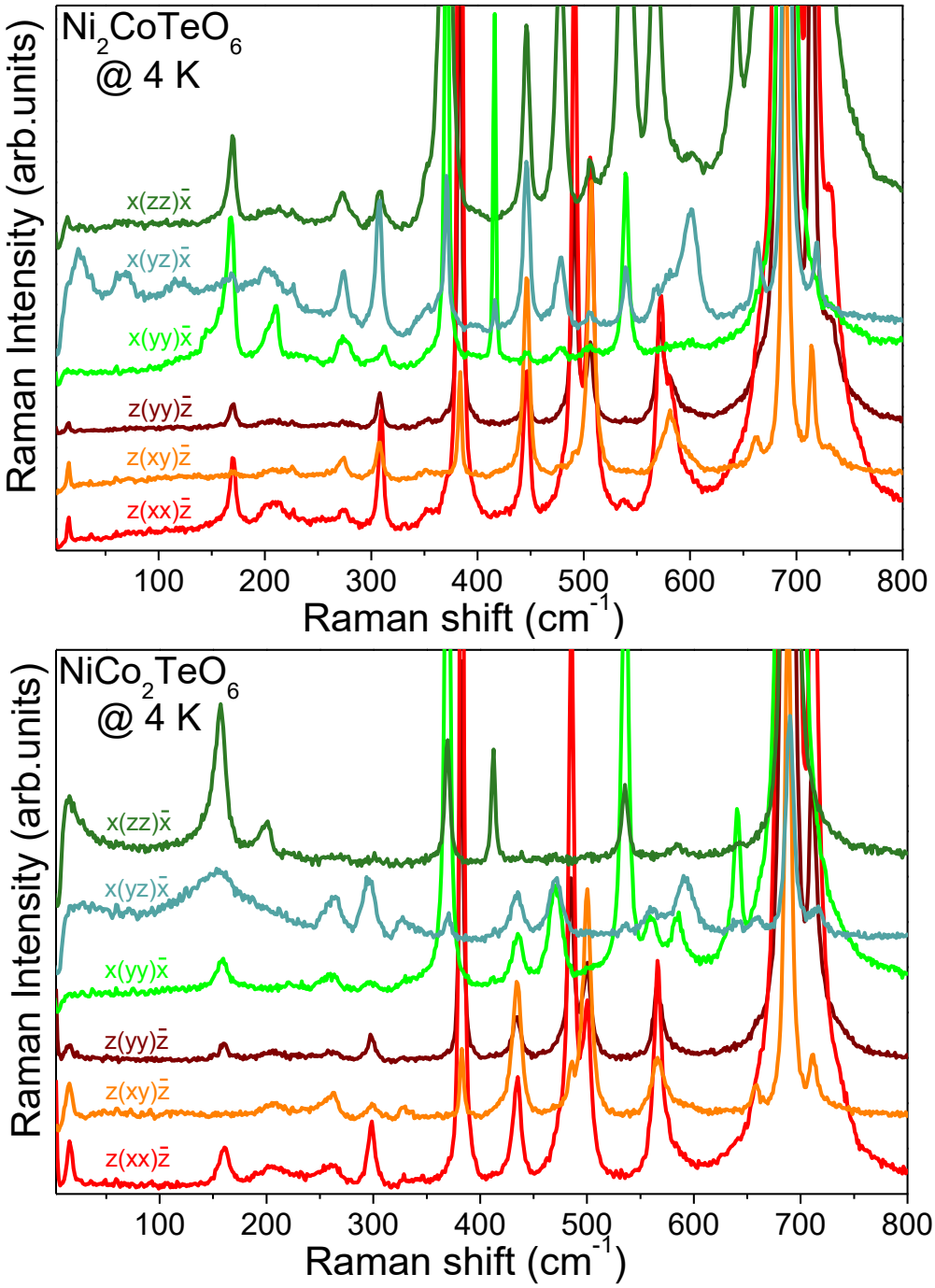

Figure S6.1.2 Raman spectra for (up) Ni_2CoTeO_6 and (down) $NiCo_2TeO_6$ single crystals, measured at 4 K and at all possible polarization configurations in the backscattering geometry. One spin excitation at ~15 cm^{-1} can be observed for both compounds.

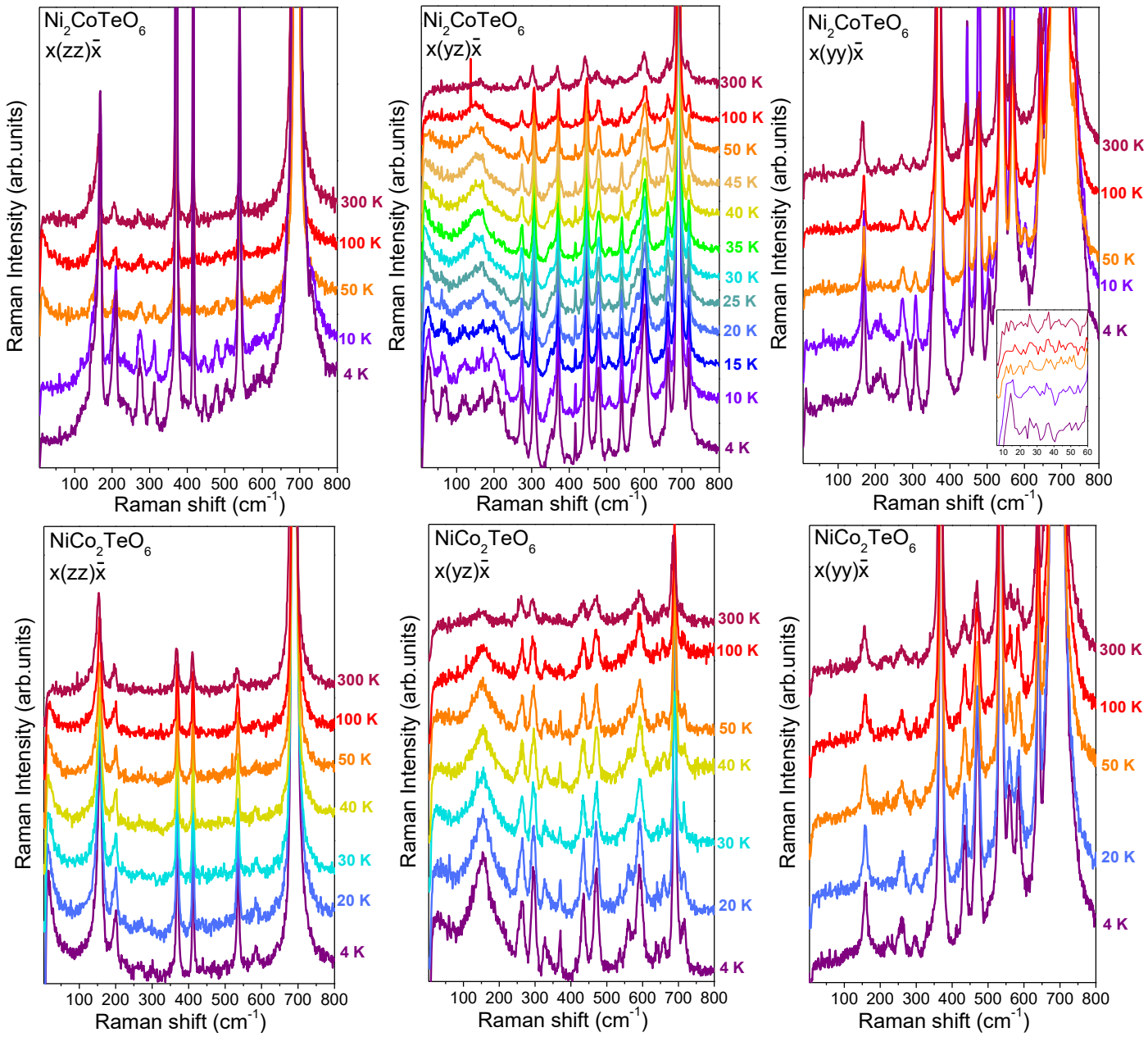

Figure S6.1.3 Temperature dependence of Raman spectra for (up) Ni_2CoTeO_6 and (down) $NiCo_2TeO_6$ single crystals, measured at $x(zz)\bar{x}$, $x(zy)\bar{x}$ and $x(yy)\bar{x}$ polarization configurations.

S6.2. Time-domain THz spectroscopy

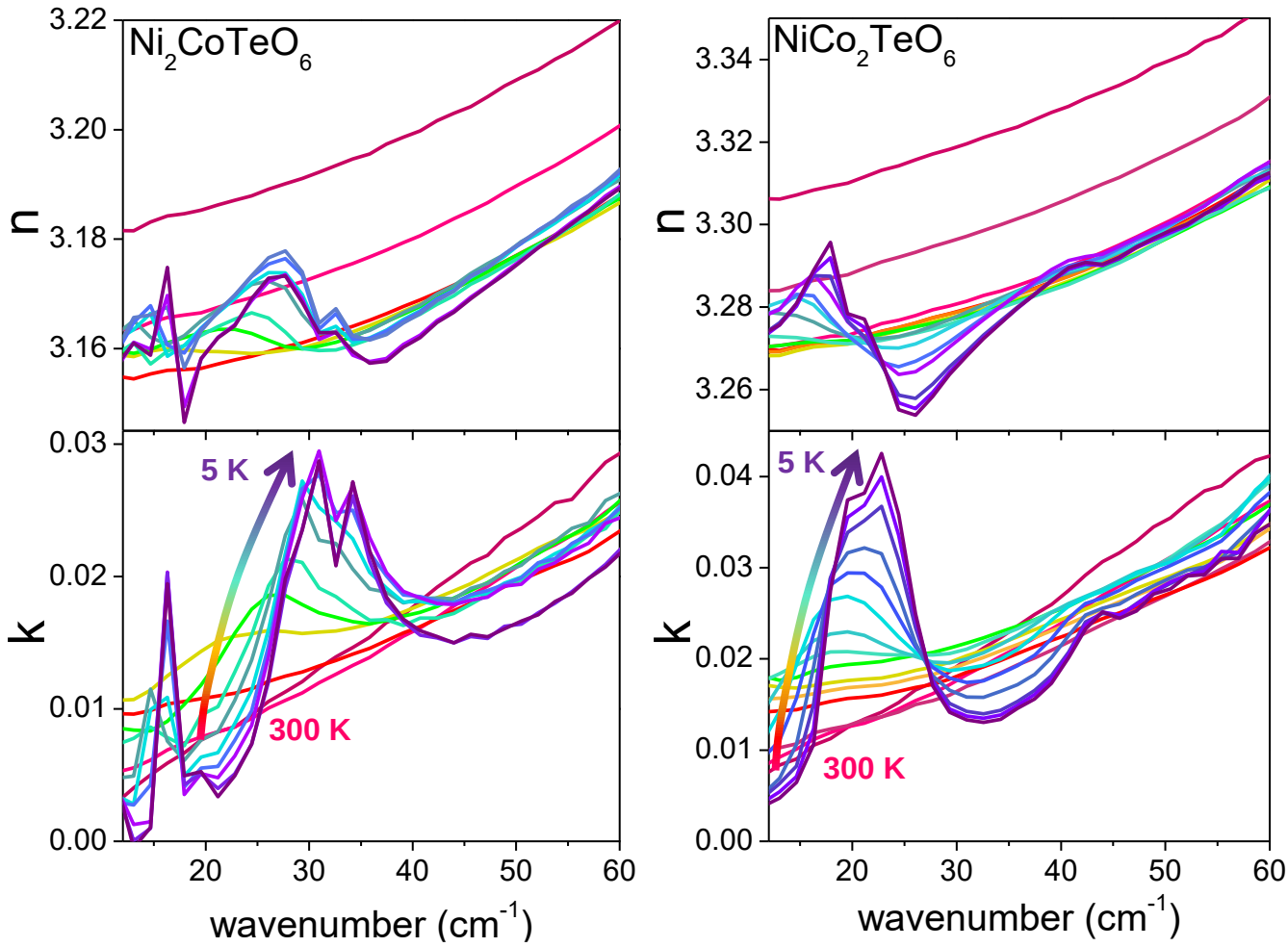

Figure S6.2.1 Temperature dependence of the real and imaginary parts of the index of refraction for (left) Ni_2CoTeO_6 and (right) $NiCo_2TeO_6$ for selected temperatures from 5 to 300 K. At least five spin excitations appear below T_N for both compounds.

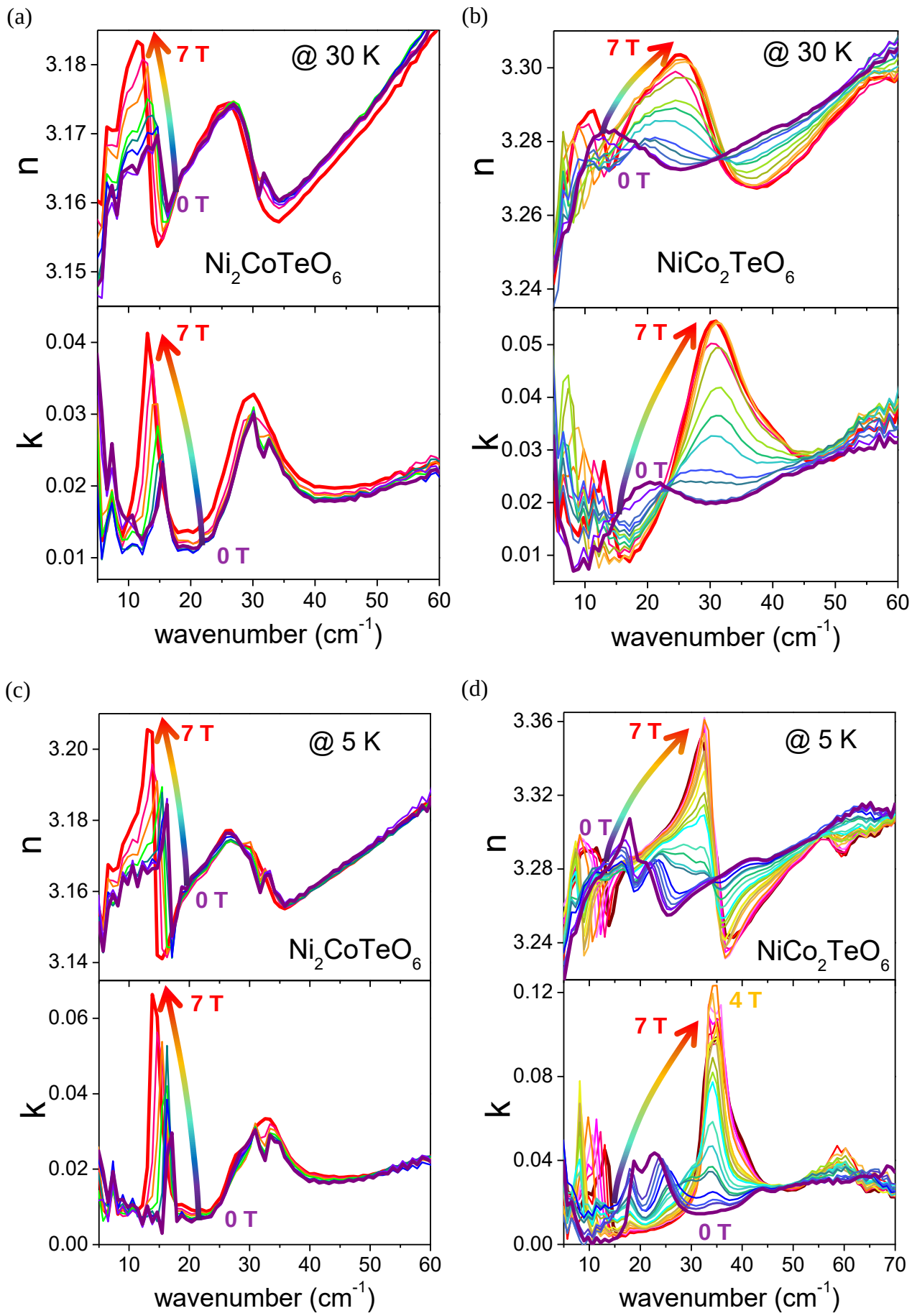

Figure S6.2.2 Magnetic field dependence of the complex index of refraction at (a), (b) 30 K, and (c), (d) 5 K of Ni_2CoTeO_6 and $NiCo_2TeO_6$ respectively, as obtained by the time-domain THz spectra, with $\boldsymbol{H}_{ext} \perp \boldsymbol{E}^{\omega}$ and up to 7 T.

S6.3. Spin and lattice excitations tables

Table S6.2.1 Frequencies of the IR active modes in the Ni_2CoTeO_6 and $NiCo_2TeO_6$ ceramics at 10 K and Raman active modes at 4 K, as obtained by the fits of IR reflectivity with ε_∞ =4.6 and 4.1 respectively. The low frequency modes in the first lines come from the THz spectra. The damping constants and dielectric strength of the IR-active modes are also listed. The modes observed as weak in Raman spectra are marked by w in subscript. Both IR- and Raman-active spin excitations are proposed to be electromagnons.

Ni_2CoTeO_6									
	Raman 4 K						IR 10 K		
Symmetry	$z(xx)\bar{z}$	$z(xy)\bar{z}$	$z(yy)\bar{z}$	$x(yy)\bar{x}$	$x(yz)\bar{x}$	$x(zz)\bar{x}$	ω_{TO}(cm^{-1})	γ_{TO}(cm^{-1})	$\Delta\varepsilon$
spin excitation	16.1	16.1	15			13.6	16.9	1.5	0.02
spin excitation					24.1		28.7	6.0	0.02
spin excitation							31.0	2.5	0.006
spin excitation							34.2	3.5	0.01
spin excitation					66.9		60.0	38.3	0.06
spin excitation					117.8				
E(TO)	171.0	162.1	169.9	167.3		168.6	165.2	13.2	0.10
							193.4	29.9	0.04
E(LO)	209.9			209.8	201.8		212.3	10.0	0.41
E(LO)	227.0$_w$	225.9$_w$	225.9$_w$		227.3	224.6$_w$	224.3	5.4	0.20
							244.4	15.4	0.16
A(TO)	274.1$_w$	274.2$_w$		272.7	274.1	272.7	269.6	12.4	0.52
							289.3	14.9	0.79
E(TO)	308.6	307.3	307.4	312.9	307.3	307.3	297.9	10.0	0.104
A(TO)	351.4$_w$	350.3$_w$	354.2$_w$		352.8	351.5	349.2	19.1	0.33
A(TO)	371.4$_w$		370.1$_w$	370.2	371.7	370.6	375.8	10.5	0.32
E(TO)	382.2	383.7	383.4						
E(LO)				415.4	415.7		424.5	33.4	0.25
E(TO)	444.9	446.4	445.9	444.8$_w$	444.8	446.3	441.7	10.5	1.17
A(TO)		475.8$_w$		477.1$_w$	478.5	477.5	446.8	6.7	0.19
A(LO)	491.5	490.6$_w$	490.4						
E(TO)	506.6	507.0	506.3	505.1$_w$	506.6$_w$	506.5	513.0	16.7	0.42
A(TO)	537.2$_w$			538.6	538.4	539.1	523.7	13.4	0.28
							530.7	7.0	0.03
E(TO)	572.0	570.5				566.7			
E(TO)	582.7	581.3	582.2		581.3$_w$	583.1$_w$	583.7	19.8	0.08
E(LO)				598.7$_w$	601.4	601.4$_w$			
A(TO)						644.1			
A(TO)	661.3				663.9	662.7			
E(TO)	689.5	689.3	688.9	690.7	691.2	690.6			
A(LO)	714.6	714.5$_w$	714.4						

$NiCo_2TeO_6$									
	Raman 4 K						IR 10 K		
Symmetry	$z(xx)\bar{z}$	$z(xy)\bar{z}$	$z(yy)\bar{z}$	$x(yy)\bar{x}$	$x(zy)\bar{x}$	$x(zz)\bar{x}$	ω_{TO}(cm^{-1})	γ_{TO}(cm^{-1})	$\Delta\varepsilon$
spin excitation							6.6	1.1	0.02
spin excitation	16.2	14.8	14.9_w				18.9	2.4	0.02
spin excitation							23.1	5.3	0.05
spin excitation							35.0	11.6	0.002
spin excitation							43.7	7.0	0.007
spin excitation							59.4	30.6	0.05
A(TO)	161.3_w		159.8_w	158.3_w	155.3_w	156.8			
E(TO)	206.1	207.7	206.2			201.6	195.2	32.7	0.43
							211.4	15.8	0.98
							237.5	15.2	0.19
							241.4	23.9	0.23
							255.1	22.7	0.83
E(TO)	263.0	263.2	262.8	261.5	263.2		278.2	18.6	0.74
E(TO)	298.8	298.9	297.4	295.9	295.8		288.4	11.2	0.09
E(LO)	328.8_w	327.3_w			327.4		320.0	11.9	0.06
A(TO)				369.1	370.6_w	369.2	345.8	38.5	0.25
E(TO)	382.7	382.7	382.7				373.2	9.9	0.37
A(TO)						412.6	413.4	31.8	0.42
E(TO)	435.0	434.9	434.5	435.0	435		428.8	12.2	1.12
A(TO)				470.9	470.9_w		433.1	6.3	0.19
E(TO)	485.8	485.7	484.8						
E(TO)	500.8	499.2	500.4				504.1	19.1	0.36
							512.7	5.3	0.01
							517.0	17.2	0.31
A(TO)				535.2		535.3			
A(TO)				559.2	559.1				
E(TO)	566.7	566.5	565.7				573.0	29.2	0.06
A(TO)				584.6	590.5				
A(LO)				639.8					
E(TO)		657.8							
E(TO)	687.8	688.3	687.9	689.2	690.0	689.5			
A(LO)	711.1	711.5_w	710.8						

References

1 G. Kresse and J. Furthmüller, Phys. Rev. B **54**, 11169 (1996).

2 J.P. Perdew, K. Burke, and M. Ernzerhof, Phys. Rev. Lett. **77**, 3865 (1996).

3 A.I. Liechtenstein, V.I. Anisimov, and J. Zaanen, Phys. Rev. B **52**, R5467 (1995).

4 M.O. Yokosuk, A. al-Wahish, S. Artyukhin, K.R. O'Neal, D. Mazumdar, P. Chen, J. Yang, Y.S. Oh, S.A. McGill, K. Haule, S.-W. Cheong, D. Vanderbilt, and J.L. Musfeldt, Phys. Rev. Lett. **117**, 147402 (2016).

5 I. Živković, K. Prša, O. Zaharko, and H. Berger, J. Phys. Condens. Matter **22**, 56002 (2010).

6 M. Rössle, C.N. Wang, P. Marsik, M. Yazdi-Rizi, K.W. Kim, A. Dubroka, I. Marozau, C.W. Schneider, J. Humlíček, D. Baeriswyl, and C. Bernhard, Phys. Rev. B **88**, 104110 (2013).